

## Enhanced Sensitivity in the VIS-NIR Range Under UV Light in a-SiC Pinpin Device

V. Silva, P. Louro, M.A. Vieira, I. Rodrigues,  
M. Vieira

Electronics Telecommunication and Computer Dept.  
ISEL – Instituto Superior de Engenharia de Lisboa  
Lisboa, Portugal

vsilva@deetc.isel.ipl.pt, plouro@deetc.isel.ipl.pt,  
mvieira@deetc.isel.ipl.pt irodrigues@deetc.isel.ipl.pt,  
mv@isel.pt

V. Silva, P. Louro, M. A. Vieira, M. Vieira

CTS-UNINOVA,  
UNL - Universidade Nova de Lisboa,  
Caparica, Portugal.

vvd.silva@campus.fct.unl.pt, plouro@deetc.isel.ipl.pt,  
mvieira@deetc.isel.pt, mv@isel.pt

**Abstract**—The use of ultra-violet (UV) steady state illumination increases the spectral sensitivity of a pi'npin photodiode beyond the visible spectrum. Increased sensitivity in the range of 400-850 nm is experimentally demonstrated. The pi'npin photodiode can be illuminated back and front sides. Under front irradiation and low power intensity the gain is high and presents a well defined peak at 750 nm and strongly quenches in the visible range. As the power irradiation increases the peak shifts to the visible range and can be deconvoluted into two peaks, one in the red range and another in the green range. Under back irradiation the gain is high in the violet/blue ranges and strongly quenches for wavelengths higher than 550 nm, whatever the intensity of the background. Results show that, front background UV illumination enhances the light-to-dark sensitivity of the medium, opening a window in the visible and near infrared range (VIS-NIR). Background illumination with UV at the back enhances only the magnitude in short wavelength range opening a window in the UV and blue ranges.

**Keywords**-UV; VIS-NIR; Visible Light Communication; SiC technology.

### I. INTRODUCTION

Light-emitting Diode (LED) is a very effective lighting technology due to its high brightness, long life, energy efficiency, durability, affordable cost, optical spectrum and its colour range for creative use. Their use as communication devices with a photo-diode as receptor, has been used for many years in hand held devices, to control televisions and other media equipment, and with higher rates, between computational devices [1]. This communication path has been used in the near infra-red (NIR) range, but due to the increasing LED lighting in homes and offices, the idea to use them for visible light communications (VLC) is present in many working groups. The Institute of Electrical and Electronics Engineers (IEEE) task group 7 has come up with the IEEE 802.15.7 VLC PHY/MAC standard proposal for the physical (PHY) and medium access control (MAC) for VLC communications [2]. The Internet use and its most popular protocols also have been studied for their performance over VLC [3]. Economic issues that will eventually guide the VLC outcome are also on the run [4].

The sensor presented in this paper, is based on amorphous silicon carbon technology (a-SiC:H) [5], it consists of a pi'npin structure. The front pi'n is thinner and has carbon a-SiC:H in the intrinsic layer while the back pin is based on a-Si:H. Two electrical optically transparent contacts interface the sensor at the front and back. Due to the asymmetric lengths of each pin structure and to their difference in materials, the sensor has interesting properties, namely a light selective filter [6]. The sensor is capable of discriminating different wavelength signals and with convenient signal modulation has the capability of logic transformations (AND, OR, NOT and XOR) over the input signals [7], which may play an important function in specific VLC applications. A multiplexing / demultiplexing function has been identified using the sensor with 4 different channels allowing WDM applications [8]. The study of UV and IR response of the sensor is important for the possible use of these wavelengths as communication channels for out-of-visible band information interchange. In this paper, we demonstrate the use of near-UV steady state illumination to increase the spectral sensitivity of the a-SiC/Si pi'npin photodiode beyond the visible spectrum. Section II describes the pi'npin structure. Section III presents the theoretical optoelectronic model and linear state equations. Section IV shows in graphical plots the experimental spectrum of the pi'npin photocurrent, and the photocurrent output for input signals in the visible and NIR spectrum ranges. Section V presents the results and their discussion. The conclusions and acknowledgement close the article.

### II. MATERIAL AND METHODS

The sensor is composed by two stacked p-i-n structures (p(a-SiC:H)- i'(a-SiC:H)-n(a-SiC:H)-p(a-SiC:H)-i(a-Si:H)-n(a-Si:H)) sandwiched between two transparent contacts at each end. The thicknesses and optical gap of the i'- (200 nm; 2.1 eV) and i- (1000 nm; 1.8 eV) layers are optimized for light absorption in the blue and red ranges [9]. The working range of the sensor is in the visible spectrum, although light sources within the ultra-violet (350-400nm) and near infra-red (700-880nm) ranges are also used.

This 1cm<sup>2</sup> structure can be seen in Figure 1, where the wavelength arrows indicate the absorption depths during operation [10] and the digital light signals  $\lambda_V, \lambda_B, \lambda_G, \lambda_R, \lambda_{IR}$ , where the V index is in the UV range, R,G,B in the Visible and IR in the NIR range.

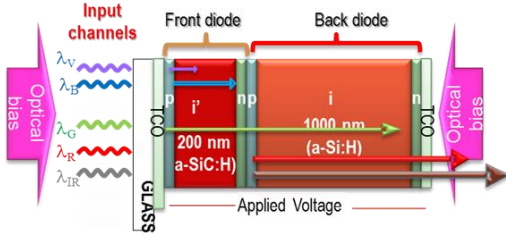


Figure 1. Device structure and operation.

General purposes LEDs are used as light sources. These light sources are used as digital signals and background lighting. The signals are impinged on the front side of the sensor. The background lighting is either at the back or at the front side. The intensity of the signal sources is very low when compared to the background intensity. The LEDs that shine on the front surface, signal and background, are set at a distance of 3cm, while the back led is almost touching the surface. Different wavelength signal sources are used: violet (400 nm), blue (470 nm), green (524 nm), red (626 nm) and infra-red (850 nm). For background lighting a 390 nm violet wavelength is applied. The signals are thus subject to constant background lighting and sampled at the midpoint of each bit. To change the background intensity different currents were used to drive the LED ( $0 < I_{LED} < 30$  mA). The sensor working point is set at -8 V.

III. THEORY

Based on the device configuration and experimental results an optoelectronic model was developed [11] and upgraded to include several inputs. The model is shown in Figure 2 as an ac equivalent circuit.

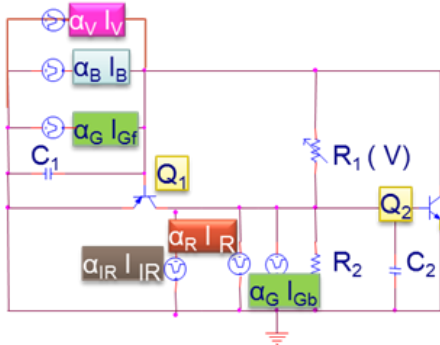


Figure 2. ac equivalent circuit of the pi-npin photodiode.

The corresponding block diagram of the ac equivalent circuit of the pi-npin photodiode, and the linear state equations, are displayed in Figure 3. Input signals,  $\lambda_{IR,R,G,B,V}$  model the input channels, and  $i(t)$  the output signal. The

amplifying elements,  $\alpha_1$  and  $\alpha_2$  are linear combinations of the optical gains of each impinging channel, respectively into the front and back phototransistors, and provide gain ( $\alpha > 1$ ) or attenuation ( $\alpha < 1$ ) depending on the background effect.

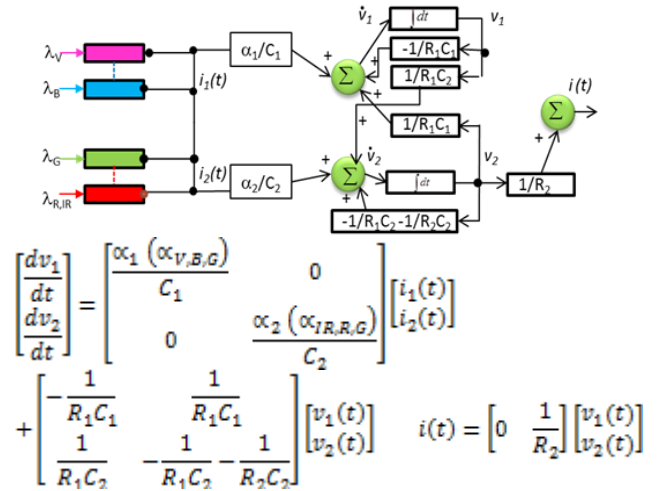


Figure 3. Block diagram and linear state equations.

The control matrix takes into account the enhancement or reduction of the channels, due to the steady state irradiation: front irradiation  $\alpha_2 \gg \alpha_1$  and back irradiation  $\alpha_1 \gg \alpha_2$ . This affects the reverse photo capacitances,  $(\alpha_{1,2} / C_{1,2})$  that determines the influence of the system input on the state change (control matrix).

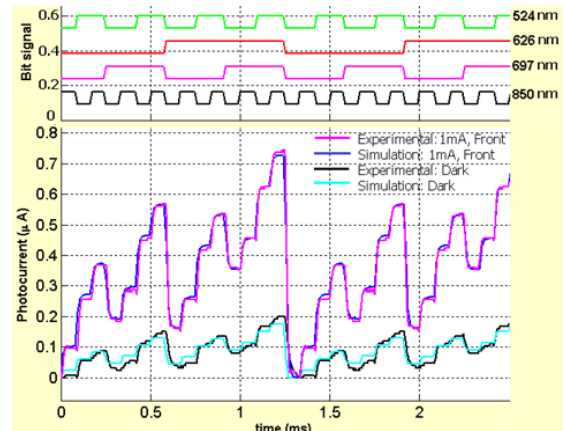


Figure 4. Simulation example of the MUX signal with and without front  $\lambda=390$  nm irradiation.

A graphics user interface (GUI) computer program was designed and programmed with MATLAB<sup>®</sup> to ease the task of numerical simulation. This interface allows the selection of model parameters, and plots the photocurrent results of the simulated and experimental data. The simulation uses as a solver, one of two alternative algorithms: a one-step solver based on an explicit Runge-Kutta formula and an implementation of the trapezoidal rule using a "free" interpolant. An example is presented in Figure 4.

IV. EXPERIMENTAL

A. Spectral measurement

Using a monochromator with 1mm slits and a chopper frequency of 3500 Hz, the spectrum measurements were made from 400 to 800 nm in 10 nm steps in three conditions: dark, front, and back. In the dark condition, the sensor is only subjected to the monochromator's light source.

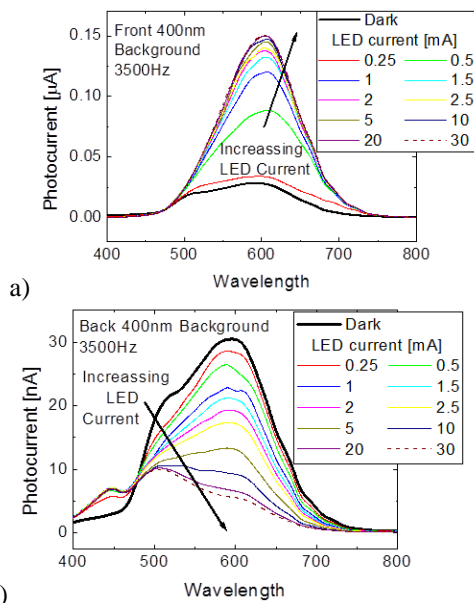


Figure 5. Photocurrent spectrum with different background lighting intensities at the a) front and b) back side of the device.

These measurements (dark) are considered as a reference. The back or front conditions refer to a steady illumination of the back or front side of the sensor.

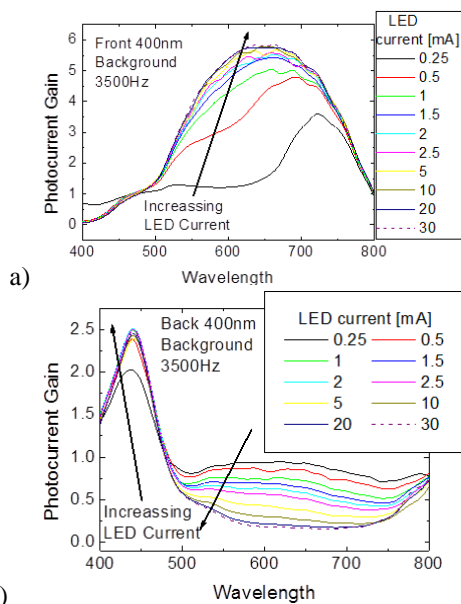


Figure 6. Photocurrent gain with a) front and b) back illumination

Several measurements were made with different background illumination intensities by applying currents in the 0.25 mA to 30 mA range, to the background LEDs with a wavelength of 400 nm. The results are presented in Figure 5.

Experimental output plotted in Figure 5a), shows that with increasing front illumination (see arrow) by the violet LED there is an increase in the gain, from 470 to 750 nm. This increase is very effective, as a current of 0.5 mA is enough to produce an output 5 times higher than the dark level, which is represented in both Figure 5a) and b) by a thick black curve. The influence of the back lighting in Figure 5b) with the same violet wavelength reduces the 470-750 nm bandwidth with increasing LED current. Photocurrent gain is defined as the ratio of the output in relation to the dark curve. The spectral gain for the different LED currents is shown in Figure 6.

B. Visible / Infrared tuning

Several monochromatic (850 nm, 697 nm, 626 nm, 524 nm, 470 nm, 400 nm) individually pulsed lights (input channels) at 12000 bps, and then combined (MUX signal), illuminated the device while steady state 390 nm bias at different intensities ( $0 < I_{LED} < 30$  mA) were superimposed separately, from either side of the sensor, and the photocurrent was measured.

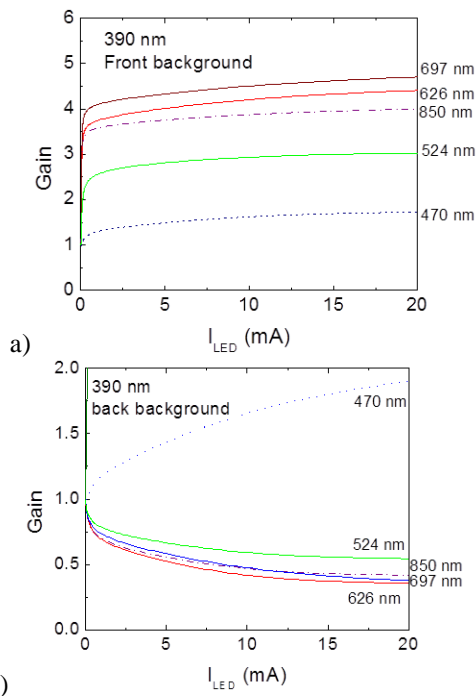


Figure 7. a) Front and b) back optical gain at  $\lambda=390$  nm irradiation and different input wavelengths.

For each individual channel the photocurrent was normalized to its value without irradiation (dark), and the photocurrent gain determined. Figure 7 displays the different gain as a function of the drive currents of the lighting LED under front and back irradiation.

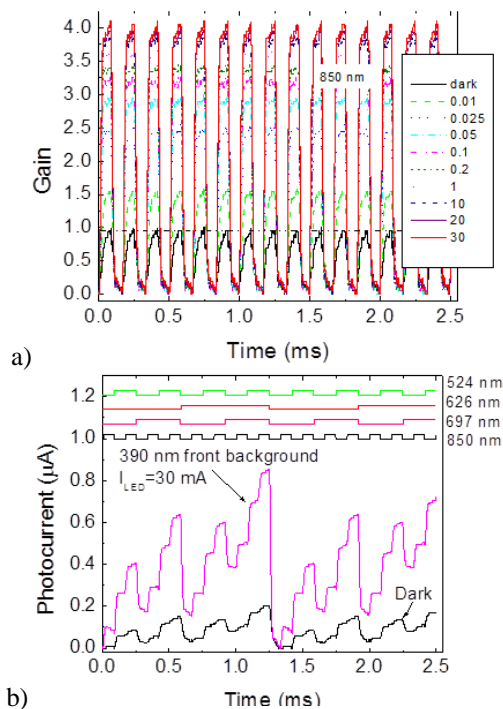


Figure 8. a) Optical gain at 390 nm front irradiation with different intensities. b) Combined polychromatic signal with and without 390 nm front irradiation and different bit sequences.

To exemplify, in Figure 8a), the gain of the 850 nm input channel, under front irradiation at different intensities, is displayed. In Figure 8b), the MUX signal due to the combination of the 850 nm, 697 nm, 626 nm and 524 nm input channels, is presented. At the top of the figure, there are the signals used to drive the input channels, and are shown to guide the eyes into the on/off states.

## V. RESULTS AND DISCUSSION

Results show, that background illumination of the front side, Figure 3a), reduces the 400-470 nm spectral range while it augments the 470-800 nm range. It acts as a selective filter for the long pass wavelengths. Background illumination of the back, Figure 3b), enhances the 400-470 nm range and reduces the 470-800 nm wavelengths. It also acts as a selective filter but for the short pass wavelengths. This fundamental behaviour is the basis of the other possible functions that can be derived from it, besides a low pass or a long pass filter. Observing the gain values of the 850 nm IR wavelength presented in Figure 7a) and b), there is a significant difference that distinguishes the background lighting at the back or front side of the device by a wavelength of 390 nm. This allows for the recovery of a NIR channel by a UV background illumination which permits a communication channel outside the visible range. The individual magnitude of each input channel without background lighting ( $I_{LED}=0$  in Figure 7), was used to simulate the input channels, and for each bit sequence shown in Figure 8b), the corresponding gain at the

simulated background intensity is presented in Figure 7. The results of the numerical simulation and the experimental results for the same sequence are presented in Figure 4, and show that a good fitting between experimental and simulated results was achieved, showing the robustness of the proposed optoelectronic model.

## CONCLUSIONS

An increased sensitivity in a SiC pi-npin device in the VIS-NIR range under UV light was experimentally and theoretically demonstrated. Results show that under front 390 nm irradiation the sensor sensitivity was enhanced in the red/infrared ranges, leading to linearly profiled collection areas that allow the incoming wavelength recognition. An optoelectronic model was presented to explain the observed data, and allow decoding of multiplexed data in the visible/infrared range. The results of the numerical simulation are coherent with the experimental results for the same input sequence.

## ACKNOWLEDGMENT

This work was supported by FCT (CTS multi annual funding) through PIDDAC Program funds and PTDC/EEA-ELC/111854/2009 and PTDC/EEA-ELC/120539/2010.

## REFERENCES

- [1] T. Komiyama, K. Kobayashi, K. Watanabe, T. Ohkubo, and Y. Kurihara, "Study of visible light communication system using RGB LED lights," in Proceedings of SICE Annual Conference, IEEE, 2011, pp. 1926-1928.
- [2] S. Rajagopal et al, "IEEE 802.15 Wireless Personal Area Networks," 2009, pp. 1-121.
- [3] V. Mai, N. Tran, T. Thang, and A. Pham, "Performance analysis of TCP over visible light communication networks with ARQ-SR protocol," 2014, pp. 1-9.
- [4] H. Chowdhury, H. Bagheri, I. Ashraf, S. Tamoore-ul-hassan, and M. Katz, "Techno-Economic analysis of Visible Light Communications," Proc. Tenth Int. Symp. Wirel. Commun. Syst. (ISWCS 2013), 2013, vol. 9, pp. 96-100.
- [5] G. De Cesare, F. Irrera, F. Lemmi, F. Palma, and M. Tucci, "a-Si:H/a-SiC:H Heterostructure for Bias-Controlled Photodetectors," MRS Proc., Feb. 2011, vol. 336, p. 885.
- [6] M. A. Vieira, "Three Transducers for One Photodetector : essays for optical communications," 2012, p. 222.
- [7] V. Silva et al, "Logic functions based on optical bias controlled SiC tandem devices," Phys. Status Solidi, vol. 11, no. 2, Feb. 2014, pp. 211-216.
- [8] M. A. Vieira, M. Vieira, P. Louro, A. Fantoni, and A. Garçon, "Demux operation in tandem amorphous Si-C devices," i-ETCISEL Acad. J. Elect. Comput., vol. 2-1, 2013, p. ID-13.
- [9] M. A. Vieira et al, "Double Pin Photodiodes with Two Optical Gate Connections for Light Triggering," Sensors & Transducers, vol. 10, no. Special issue, 2011, pp. 96-120.
- [10] A. Fantoni, M. Vieira, and R. Martins, "Simulation of hydrogenated amorphous and microcrystalline silicon optoelectronic devices," Math. Comput. Simul., vol. 49, no. 4-5, Sep. 1999, pp. 381-401.
- [11] M. Vieira, P. Louro, M. Fernandes, and M. A. Vieira, "Three Transducers Embedded into One Single SiC Photodetector," in Advances in Photodiodes, vol. March Ch19, G. F. D. Betta, Ed. Intech, 2011, pp. 403-426.